Theor Chem Acc (2012) 131:1100
DOI 10.1007/s00214-012-1100-7

REGULAR ARTICLE

Mechanistic and kinetic study the reaction of $O(^3P)$ + CH_3CFCH_2

Yunju Zhang · Jingyu Sun · Kai Chao · Hao Sun · Fang Wang · ShuWei Tang · Xiumei Pan · Jingping Zhang · Rongshun Wang

Received: 24 March 2011 / Accepted: 27 July 2011 / Published online: 2 March 2012

Abstract The triplet potential energy surface of the $O(^3P)$ + CH_3CFCH_2 reaction has been investigated at the BMC-CCSD//MP2/6-311++G(d,p) level. Multichannel RRKM theory and transition state theory are employed to calculate the rate constants over a wide range of temperatures and pressures. The total rate constants show positive temperature dependence and pressure independence. At pressure of 10 Torr with He as bath gas, the addition/elimination on triplet potential energy surface is a dominant pathway. Major predicted end products are CH_3CFCHO (I) and H at the temperatures between 200 and 3,000 K; the direct hydrogen abstraction leading to OH + CH_2CFCH_2(I) plays an important role at higher temperatures. The calculated overall rate constants are in good agreement with the available experimental data.

Keywords CH_3CFCH_2 · $O(^3P)$ · Mechanism · Rate constants

Electronic supplementary material The online version of this article (doi:10.1007/s00214-012-1100-7) contains supplementary material, which is available to authorized users.

Y. Zhang · J. Sun · K. Chao · H. Sun · F. Wang · S. Tang · X. Pan · J. Zhang · R. Wang (✉)
Institute of Functional Material Chemistry,
Faculty of Chemistry, Northeast Normal University,
Renmin Road 5268, Changchun 130024,
Jilin, People's Republic of China
e-mail: wangrs@nenu.edu.cn

H. Sun
Institute of Theoretical Chemistry, State Key Laboratory of Theoretical and Computational Chemistry, Jilin University, Changchun 130023, Jilin, People's Republic of China

1 Introduction

Chlorofluorocarbons (CFCs) can cause depletion of the stratospheric ozone layer as well as global warming. Therefore, international researchers were prompted to find the replacement with environmentally friendly alternatives for CFCs [1, 2]. Hydrofluorocarbons (HFCs) contain neither chlorine nor bromine and hence do not contribute to stratospheric ozone depletion [3]. In recent years, HFCs have been of interest as possible substitutes for the ozone-depleting CFCs. However, HFCs still have the potential contributions to the global warming effect because of their infrared absorbing properties of such fluorinated compounds. Therefore, it is necessary to know the atmospheric lifetime to access environmental impact and possible global warming effects. Because the unsaturated HFCs introduction of C=C bond may lead to an even greater reactivity, decreased atmospheric lifetime, and global warming potentials (GWP) of HFCs, unsaturated HFCs are considered to be the promising substitutes of CFCs. In order to evaluate the atmospheric lifetimes and the environmental assessment of unsaturated HFCs, investigating the reactivity of unsaturated HFCs against the O atom and accurate data for their reaction rate constants as well as their temperature and pressure dependence are required and important. Such reactions of unsaturated HFCs with free radicals had been extensively studied experimentally and theoretically [4–18]. In this study, we will pay attention to the reactions of CH_3CFCH_2 with $O(^3P)$.

In previous studies, the reaction of $CHF=CH_2$ [14] $CF_2=CF_2$ [15] $CH_3CF=CH_2$ [16] $CF_3CH=CH_2$ [16–18] $CF_3CF=CF_2$ [16, 17] with $O(^3P)$ had been extensively studied in experiment. Except for the reaction of $O(^3P)$ with $CF_2=CF_2$, the rate constant of $O(^3P)$ with other fluorinated olefins decreased with the increasing number of

fluorine substituted [16] compared with unsubstituted alkenes, which may be due to strong electron withdrawing effect of F atom. However, the reaction of $O(^3P)$ with CH_3CFCH_2 has only been studied by one research group [19]. They have measured the rate constant at 298 K, and the rate constant is $k = 1.99 \times 10^{-12}$ cm^3 molecule^{-1} s^{-1}. To our knowledge, there are no theoretical studies on the reactivity of $O(^3P)$ with CH_3CFCH_2. In this article, we report the first detailed theoretical study on the triplet potential energy surface and rate constants over a wide temperatures and pressures for the title reaction, applying the TST and multichannel RRKM theories. For the title reaction, the following product channels are revealed for the first time, that is,

$$\begin{aligned} CH_3CFCH_2 + O(^3P) &\rightarrow CH_2CFCH_2 + OH\ (1)\\ &\rightarrow CH_3CFCH + OH\ (2)\\ &\rightarrow CH_3CFCHO + H\ (3)\\ &\rightarrow CH_3CF + CH_2O\ (4)\\ &\rightarrow CH_3CHF + HCO\ (5)\\ &\rightarrow CH_3CFCOH + H\ (6)\\ &\rightarrow CH_2CHF + HCOH\ (7)\\ &\rightarrow CH_2CFOH + CH_2\ (8)\\ &\rightarrow CH_2COF + CH_3\ (9)\\ &\rightarrow CH_3COF + CH_2\ (10). \end{aligned}$$

2 Computational methods

All the electronic structure calculations are carried out using GAUSSIAN 03 programs [20]. The geometries of all species for the $O(^3P) + CH_3CFCH_2$ reaction are first optimized using the MP2 method [21] with the 6-311++G(d,p) basis set. The harmonic vibrational frequencies are obtained at the MP2/6-311++G(d,p) level to characterize the minimum or first-order transition state. Connections of the transition states between two local minima have been confirmed by intrinsic reaction coordinate (IRC) calculations [22, 23]. The geometries optimized at the MP2/6-311++G(d,p) are used to perform single-point energy calculations for all species using the BMC-CCSD method [25]. In this work, we have also carried out the calculations using CCSD(T)/6-311++G(d,p) [24], G3(MP2) [26], and CCSD(T)/aug-cc-pVTZ [27] methods in order to test the accuracy of BMC-CCSD energies. In view of two aspects in the accuracy of the calculations at the BMC-CCSD level: (1) The mean unsigned error for barrier height is only 0.71 kcal/mol [43], and (2) the rate constant is determined mainly by the barrier height and the calculated entrance barrier of 0.89 kcal/mol, which is smaller than the two latter methods. It has been shown that the BMC-CCSD method gives accurate energetics for many reactions [28–30]. To gain an insight on multireference character for the stationary points, the T_1 diagnostic is monitored for each point using the CCSD(T)/6-311++G(d,p) method. Values of closed-shell systems exceeding 0.02 are suspected. Meanwhile, T_1 diagnostic values of open-shell system up to 0.045 may be accepted [31–34]. Fortunately, the T_1 values of closed-shell and open-shell species in our system are smaller than 0.02 and 0.045, which means that multireference character in the CCSD wave functions is not a problem.

The rate constants for the main product channels of the $O(^3P) + CH_3CFCH_2$ reaction have been calculated with transition state theory (TST) and multichannel RRKM theory. In fact, RRKM–TST method has been successfully used to deal with many bimolecular reactions in which the unimolecular decomposition of energy-rich adduct occurs [35–37]. In the present kinetic calculations, we used a modified computer program written for the $C_2H_5CO + O_2$ reaction by Hou and Wang [37].

3 Results and discussion

For the $O(^3P) + CH_3CFCH_2$ reaction, the optimized structures of the reactants and products are shown in Fig. 1, along with the available experimental values. It can be seen from Fig. 1 that the calculated bond lengths of product species are in good agreement with experimental values. Figure 2 depicts the optimized structures of intermediates and transition states. The schematic triplet potential energy surface for the title reaction is plotted in Fig. 3 to clarify the reaction mechanisms. Table 1 summarizes the ZPE corrections, T_1 diagnostic values, relative energies, and reaction enthalpies of all species found on the PES. The harmonic vibrational frequencies and atomic Cartesian coordinates of the key species are listed in Table S1 and S2, respectively. The moment of inertia and rotational symmetry numbers of all the species are shown in Table S3 as supplementary materials. In the following discussion, the MP2/6-311++G(d,p) optimized geometric parameters and the BMC-CCSD + ZPE energies are used unless otherwise stated.

3.1 Direct hydrogen abstraction

As shown in Scheme 1, there are four distinct chemical environments of hydrogen atoms in CH_3CFCH_2. They are vinyl terminal hydrogen (two out-of-plane H atoms H_a and the in-plane H atom H_b) and allylic hydrogen (H_c and H_d). Therefore, four transition states are located for atomic oxygen abstracting the H atoms in CH_3CFCH_2 to form OH radical. In the C_s symmetry CH_3CFCH_2 molecule, three hydrogen atoms in methyl are not equivalent, as stated

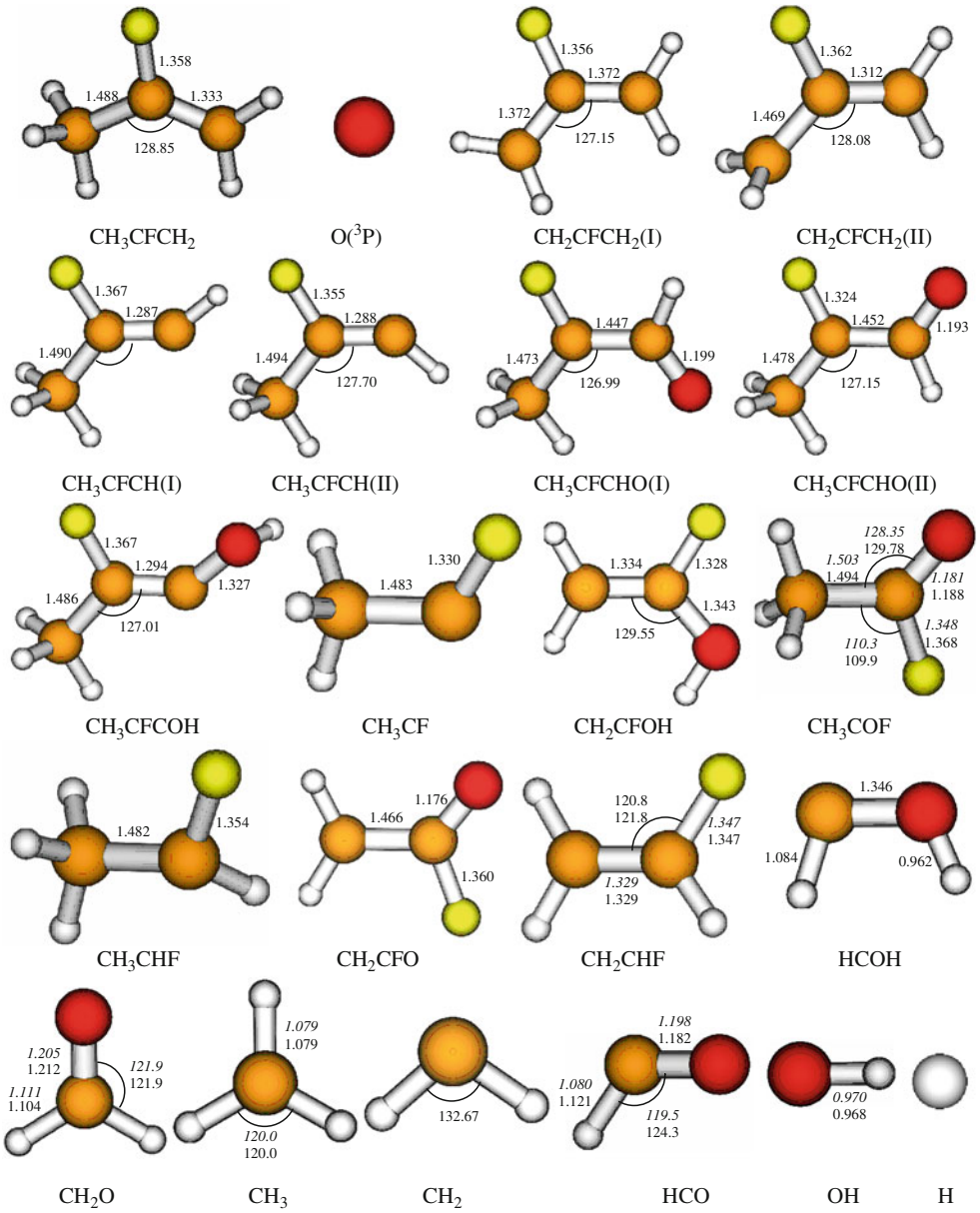

Fig. 1 The optimized structures of the reactants and products for the reaction of $O(^3P)$ with CH_3CFCH_2 at the MP2/6-311++G(d,p) level. Distances are given in angstroms and angles are in degrees. The values in *italics* are experimental data from ref. [44]

earlier, two H atoms out-of-plane and one H atom in-plane. TS1a and TS2a are the corresponding transition states to form P1 (CH_2CFCH_2(I) + OH) and P2 (CH_2CFCH_2(II) + OH), respectively. In TS1a and TS2a, the new forming O–H bond in TS1a and TS2a is about 1.22 and 1.18 Å, which are about 0.25 and 0.21 Å longer than that in OH radical, respectively. The breaking C–H bonds are as long as 1.26 and 1.28 Å, about 0.17 and 0.19 Å longer than the equilibrium distance in reactants. The elongation of the forming bond is longer than that of the breaking bond, and therefore, TS1a and TS2a are reactant-like transition states, and the channels proceed via an early barrier. It is noted that CH_2CFCH_2(I) and CH_2CFCH_2(II) are conformers. However, CH_2CFCH_2(I) has a C=C=C double–double-bond-like structure, and all atoms are in the plane $CCCH_c$. CH_2CFCH_2(II) has a C=C double-bond-like structure and a C–C single-bond-like structure where two out-of-plane H atoms H_a are located symmetrically on the two sides of the $CCCH_c$ plane as depicted in Fig. 1. The energy of CH_2CFCH_2(I) is 17.6 kcal/mol lower than that of CH_2CFCH_2(II) at the BMC-CCSD//MP2/6-311++G(d,p) level. Furthermore, the formation of P1 (CH_2CFCH_2(I) + OH) is exothermic by 13.3 kcal/mol, whereas the formation of P2 (CH_2CFCH_2(II) + OH) is 4.4 kcal/mol endothermic, and the barriers of TS1a and TS2a are 8.4 and 13.2 kcal/mol, respectively. Obviously, CH_2CFCH_2(I) is more stable than CH_2CFCH_2(II). These results indicate that the formation of P1 (CH_2CFCH_2(I) + OH) channel by H-migration is favorable than that of P2 (CH_2CFCH_2(II) + OH).

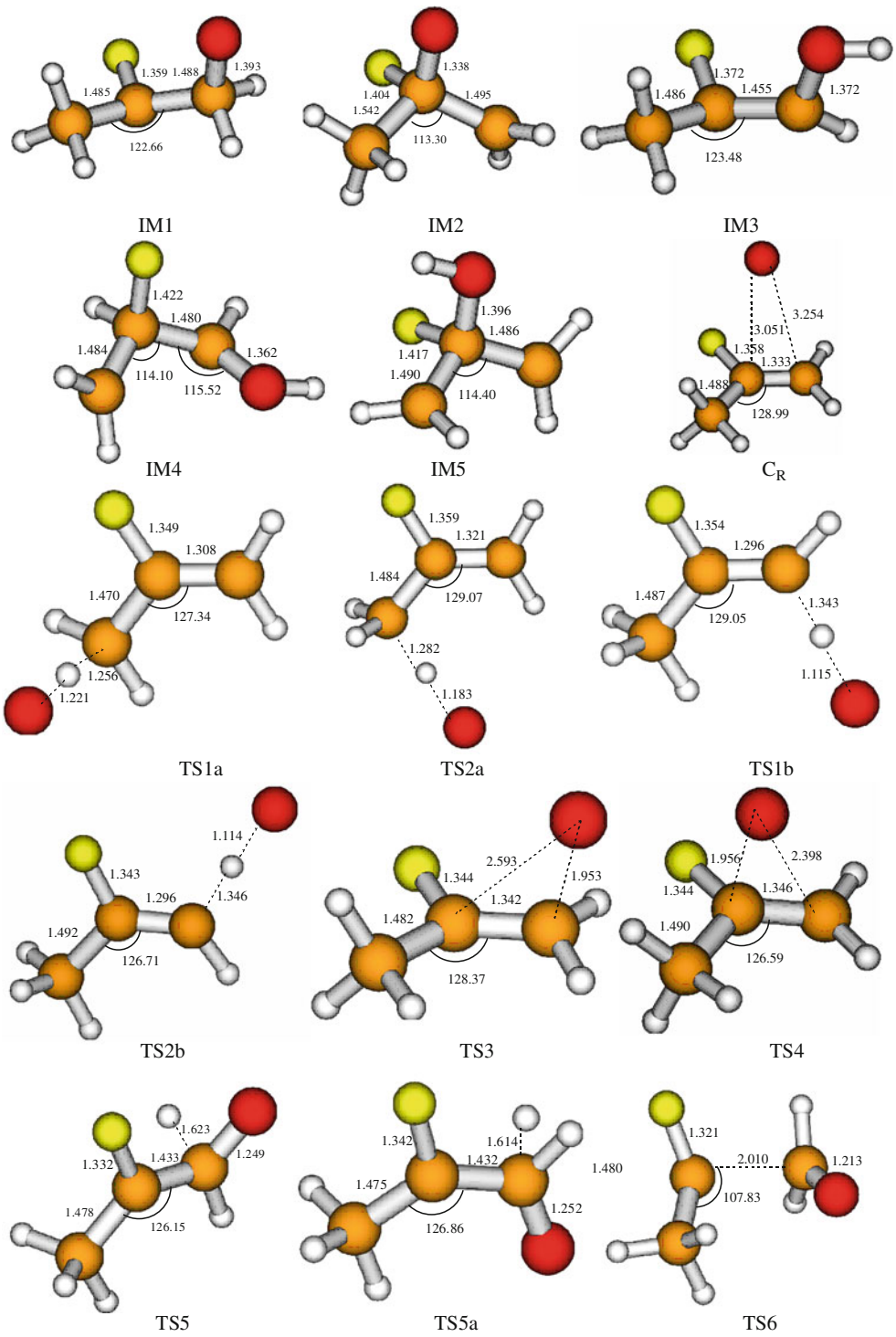

Fig. 2 The optimized structures of intermediates and transition states for the reaction of $O(^3P)$ with CH_3CFCH_2 at the MP2/6-311++G(d,p) level. Distances are given in angstroms and angles are in degrees

The atomic $O(^3P)$ can abstract the H atom in CH_2 (H_c and H_d) group to P3 ($CH_3CFCH(I) + OH$) and P4 ($CH_3CFCH(II) + OH$). TS1b and TS2b are the corresponding transition states. In TS1b, the breaking C–H bond is stretched by 0.26 Å compared with the equilibrium distance of C–H bond in $CH_3CFCH(I)$; the forming O–H bond is about 0.15 Å longer than that in OH radical. Therefore, in view of structure, TS1b is product-like transition state. Similar conclusions take place for TS2b. However, two channels are both endothermic. The barrier heights of TS1b and TS2b are about 16.0 and 16.6 kcal/mol, which is 7.6 and 8.2 kcal/mol higher than that of TS1a, respectively. Thus, the endothermic products P3 and P4 can only be reached at very high temperatures.

Fig. 2 continued

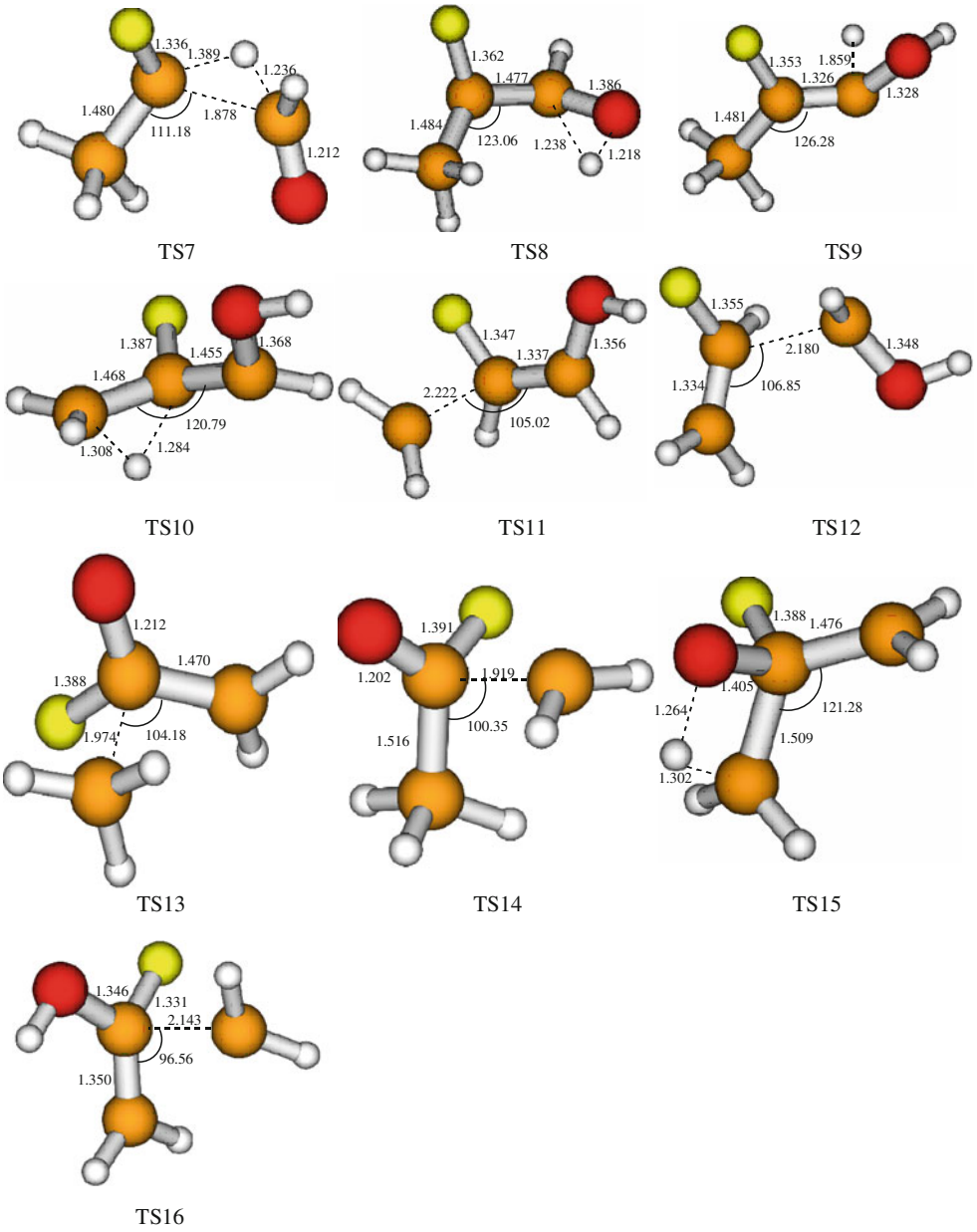

In view of barrier heights and reaction enthalpies, the hydrogen abstraction from vinyl terminal hydrogen (the two out-of-plane H atoms H_a) is more favorable than other abstraction pathways.

3.2 Addition/elimination

3.2.1 Entrance channel

The interaction between the O(^{3}P) and C=C double bond of CH_3CFCH_2 forms a pre-reaction complex C_R ($O\cdots C_3H_5F$). The addition of O(^{3}P) radical can occur at both carbon atoms of the double bond. When the O(^{3}P) radical attacks the terminal C of CH_3CFCH_2 in the double bond, the intermediate IM1 (CH_3CFCH_2O) is formed via TS3 lying above the reactant by 0.9 kcal/mol with a barrier of 1.9 kcal/mol. On the other hand, if the O(^{3}P) radical is added to the central C of the CH_3CFCH_2, the intermediate IM2 ($CH_3CF(O)CH_2$) is formed via TS4 lying above the reactant by 1.7 kcal/mol with a potential energy barrier of 2.7 kcal/mol. The processes of forming the intermediate IM1 and IM2 are typical O-addition mechanisms due to the rich electron double bond in CH_3CFCH_2 and the strong electronegativity of O atom. IM1 and IM2 are 21.3 and 30.5 kcal/mol more stable than the reactant, which means that the initial association provides IM1 and IM2 with

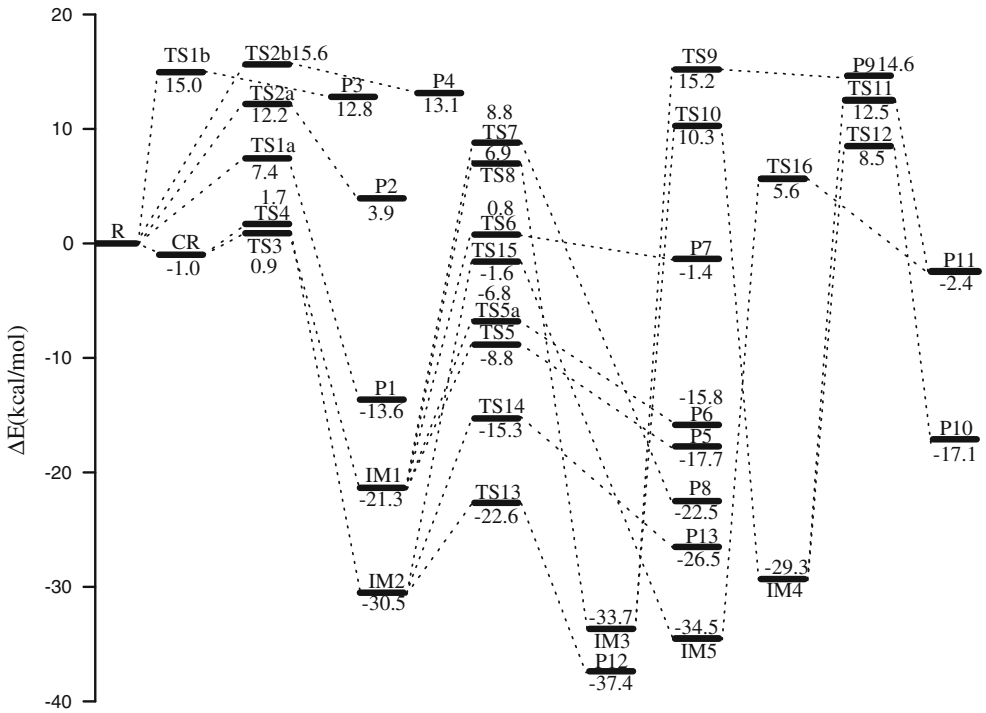

Fig. 3 The profile of potential energy surface for the $O(^3P) + CH_3CFCH_2$ reaction. The relative energies are calculated at the BMC-CCSD//MP2/6-311++G(d,p) + ZPE level of theory

enough energy to take subsequent changes. In the following, we will discuss the formation pathways of various products from IM1 and IM2.

3.2.2 *Decomposition of IM1 [CH_3CFCH_2O]*

Four decomposition pathways from IM1 have been found. The energetically most favorable reaction path involves the formation of P5 (CH_3CFCHO (I) + H) via the C–H bond cleavage transition state TS5. The barrier height for this channel is calculated to be 12.5 kcal/mol at the BMC-CCSD level. The second pathway is initiated by dissociation of the C–H bond to give formally P6 (CH_3CFCHO (II) + H) via transition state TS5a. The barrier height is 14.5 kcal/mol, which is 2.0 kcal/mol higher than TS5. Furthermore, TS5 and TS5a have very similar vibration frequencies and geometrical parameters. The classical barrier height (i.e., without the ZPE correction) is calculated to be 17.0 kcal/mol for TS5. It is conceivable that the ZPE might play an important role in TS5. As shown in Table 1, TS5 has almost the smallest ZPE and the largest ZPE difference with respect to the reactants (e.g., $\Delta ZPE_{TS5} = -3.1$ kcal/mol). Similar conclusions take place for TS5a.

The third reaction channel of IM1 produces P7 ($CH_3CF + CH_2O$) via the C–C bond fission transition state TS6 after clearing a barrier of 22.1 kcal/mol height. However, TS6 is still higher than TS5 by 9.6 kcal/mol and TS5a by 7.6 kcal/mol. Moreover, the predicted heat of reaction for the formation of P7 is −0.9 kcal/mol, which is higher than that of P5 (CH_3CFCHO (I) + H) by 17.7 kcal/mol and that of P6 (CH_3CFCHO (II) + H) by 15.8 kcal/mol; this is reasonable, as the C–C bond dissociation energy is greater than that of C–H bond [38]. These results indicate the formation of P7 channel is far from competitive with that of P5 and P6 pathways under normal conditions. The last examined decomposition pathway is to produce P8 ($CH_3CHF + HCO$) by breaking the C–C bond along with the H in the center carbon of IM1 migration to the oxygen-bonded carbon atom along with the reaction exothermicity of 22.0 kcal/mol. However, the barrier height, 30.1 kcal/mol, is rather high, indicating that the formation of product P8 is not important to the overall reaction.

3.2.3 *Isomerization channel of IM1 [CH_3CFCH_2O]*

TS8 is the transition state for hydrogen migration from the oxygen-bonded carbon atom to the oxygen atom, forming another intermediate IM3 ($CH_3CFCHOH$). TS8 is a three-membered-ring structure. The breaking C–H bond is elongated to 1.24 Å. The forming H–O bond is 1.22 Å. It should be pointed out that the process IM1 → IM3 is kinetically less feasible at normal temperatures. However, because their conversion barrier is just 6.9 kcal/mol above the reactant, this conversion may become feasible at higher temperatures. Once such a higher-energy transition state TS8 is surmounted, subsequently, several reaction pathways can take place. First, IM3 can directly be decomposed to yield P9 ($CH_3CFCOH + H$) via a transition state TS9 after clearing a high barrier of 48.9 kcal/mol. The product P9 ($CH_3CFCOH + H$) is about 14.6 kcal/mol higher than

Table 1 ZPE corrections, T_1 diagnostic values, and relative energies for various species as well as relative enthalpies of intermediates and products at 298 K (energies in kcal/mol)

Species	ZPE	T_1[a]	ΔE[b]	ΔE[c]	ΔE[d]	ΔE[e]	ΔH[f]	ΔH[g]	ΔH[h]	ΔH[i]
R: $CH_3CFCH_2 + O(^3P)$	45.6	0.012, 0.008	0.0	0.0	0.0	0.0	0.0	0.0	0.0	0.0
P1: CH_2CFCH_2(I) + OH	42.3	0.025, 0.010	−13.6	−18.1	−7.9	−11.2	−17.7	−13.3	−7.5	−10.8
P2: CH_2CFCH_2(II) + OH	43.9	0.016, 0.010	3.9	−1.5	8.3	5.6	−1.0	4.4	8.8	6.1
P3: CH_3CFCH(I) + OH	43.6	0.026, 0.010	12.8	8.4	17.9	15.4	8.9	13.3	18.4	15.8
P4: CH_3CFCH(II) + OH	43.6	0.026, 0.010	13.1	8.5	18.0	15.4	9.0	13.6	18.5	16.0
P5: $(CH_3CFC(O)H$(I) + H)	41.1	0.023, 0.000	−17.7	−22.6	−11.1	−13.8	−22.0	−18.6	−11.9	−14.6
P6: $(CH_3CFC(O)H$(II) + H)	41.2	0.024, 0.000	−15.8	−20.4	−8.7	−11.5	−19.8	−16.7	−9.6	−12.4
P7: $(CH_3CF + CH_2O)$	43.7	0.016, 0.017	−1.4	−6.4	1.4	0.5	−6.00	−0.9	1.8	0.9
P8: $(CH_3CHF + HCO)$	42.7	0.014, 0.024	−22.5	−27.1	−18.8	−20.1	−26.6	−22.0	−18.2	−19.6
P9: $(CH_3CFCOH + H)$	42.0	0.026, 0.000	14.6	11.1	22.8	19.7	11.7	13.7	21.8	18.8
P10: $(CH_2CHF + HCOH)$	43.0	0.013, 0.018	−17.1	−19.8	−10.8	−15.4	−22.4	−19.6	−13.0	−17.6
P11: $(CH_2CFOH + CH_2)$	41.4	0.013, 0.009	−2.4	−6.6	14.8	0.6	−5.8	−1.8	13.2	−1.1
P12: $(CH_2COF + CH_3)$	41.9	0.020, 0.008	−37.4	−41.9	−31.6	−34.5	−41.1	−36.6	−30.8	−33.7
P13: $(CH_3COF + CH_2)$	40.4	0.018, 0.009	−26.5	−31.8	−12.6	−15.6	−31.1	−25.8	−17.5	−24.2
CR1($O^{\cdots}C_3H_5F$)	46.0	0.011	−1.00	−0.9	−1.1	−1.2	−0.8	−0.9	−1.0	−1.1
IM1(CH_3CFCH_2O)	46.9	0.017	−21.3	−19.1	−17.6	−20.9	−19.7	−21.9	−18.2	−21.5
IM2($CH_3CF(O)CH_2$)	46.1	0.017	−30.5	−28.1	−26.6	−29.7	−28.8	−31.2	−27.2	−30.3
IM3($CH_3CFCHOH$)	47.2	0.017	−33.7	−29.4	−26.4	−30.5	−29.9	−34.1	−26.8	−31.0
IM4($CH_2CHFCHOH$)	46.3	0.016	−29.3	−25.1	−22.2	−26.3	−25.4	−29.6	−22.5	−26.6
IM5($CH_2CF(OH)CH_2$)	45.0	0.014	−34.5	−30.7	−27.8	−31.9	−31.0	−34.8	−28.1	−32.2
TS1a	42.8	0.024	7.4	10.9	12.3	9.2				
TS2a	43.2	0.016	12.2	14.5	15.9	12.7				
TS1b	42.7	0.024	15.0	18.4	20.2	16.8				
TS2b	42.6	0.024	15.6	19.2	20.9	17.7				
TS3	46.5	0.027	0.9	11.7	4.8	1.4				
TS4	46.3	0.028	1.7	4.5	6.0	2.6				
TS5	42.5	0.024	−8.8	−5.2	−1.5	−5.9				
TS5a	42.6	0.025	−6.8	−3.0	0.6	−3.7				
TS6	45.5	0.026	0.8	4.6	7.4	3.7				
TS7	44.2	0.023	8.8	12.3	16.3	11.6				
TS8	44.4	0.018	6.9	10.7	14.0	8.9				
TS9	42.6	0.025	15.2	19.4	23.7	19.0				
TS10	44.3	0.018	10.3	15.4	19.9	14.4				
TS11	43.9	0.026	12.5	17.4	20.9	16.3				
TS12	44.8	0.027	8.5	13.7	17.1	12.6				
TS13	44.2	0.023	−22.6	−19.1	−15.8	−20.1				
TS14	44.5	0.022	−15.3	−12.0	−9.3	−12.9				
TS15	42.9	0.018	−1.6	2.2	5.3	0.1				
TS16	43.5	0.024	5.6	11.1	15.1	9.8				

[a] T_1 diagnostic values are calculated at the CCSD(T)/6-311++G(d,p) level

[b] At the BMC-CCSD + ZPE level

[c] At the G3(MP2) + ZPE level

[d] At the CCSD(T)/6-311++G(d,p) + ZPE level

[e] At the CCSD(T)/aug-cc-pVTZ + ZPE level

[f] The calculated heats of reaction at 298 K at the G3(MP2) level

[g] The calculated heats of reaction at 298 K at the BMC-CCSD level

[h] The calculated heats of reaction at 298 K at the CCSD(T)/6-311++G(d,p) level

[i] The calculated heats of reaction at 298 K at the CCSD(T)/aug-cc-pVTZ level

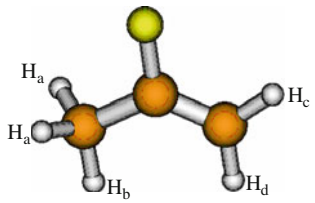

Scheme 1 The four different chemical H atoms in CH_3CFCH_2

reactants. Apparently, the pathway is of no importance for the whole reaction. Second, the hydrogen atom of the terminal CH_3 group can shift to the center carbon atom in IM3 leading to IM4 ($CH_2CHFCHOH$) via TS10 with a barrier of 44.0 kcal/mol. IM4, −29.3 kcal/mol relative to the initial reactant, can dissociate to the product P10 ($CH_2CHF + HCOH$) and P11 ($CH_2CFOH + CH_2$) by breaking the C–C bond, respectively. The corresponding barrier heights are 37.8 and 41.8 kcal/mol, respectively. Due to higher barriers, the channels which initiated from IM3 are expected to be negligible at low and moderate temperatures.

3.2.4 Decomposition of IM2 [$CH_3CF(O)CH_2$]

As seen from Fig. 3, two possible decomposition channels of IM2 are found. The most feasible decomposition channel of IM2 is the formation of P12 ($CH_2COF + CH_3$) via the C–C bond fission transition state TS13 with a barrier of 7.9 kcal/mol. The breaking C–C bond in TS13 is 1.97 Å, which is 0.43 Å longer than that in the IM2. It is anticipated that dissociation step passes an early barrier, which is in accordance with the reaction exothermicity of 36.6 kcal/mol. In addition, the formation of P12 ($CH_2COF + CH_3$) is the most stable product on the PES. The second decomposition channel is the C–C bond fission in IM2 leading to P13 ($CH_3COF + CH_2$) via TS14 overcoming a barrier of 15.2 height, which is exothermicity by 25.8 kcal/mol. However, TS14 is still higher than TS13 by 7.3 kcal/mol. These results indicate that the formation of P12 ($CH_2COF + CH_3$) is more favorable than the formation of P13 ($CH_3COF + CH_2$).

3.2.5 Isomerization channel of IM2 [$CH_3CF(O)CH_2$]

IM2 can rearrange to intermediate IM5 ($CH_2CF(OH)CH_2$) via a four-center transition state TS15, needing to surmount a barrier of 28.9 kcal/mol. Subsequently, the C–C bond dissociation in IM5 could produce P11 ($CH_2CFOH + CH_2$). The corresponding barrier height is 40.1 kcal/mol. Moreover, the formation of P11 ($CH_2CFOH + CH_2$) is only exothermic by 1.8 kcal/mol. Therefore, it should be anticipated that this channel should play a negligible role in the reaction.

In summary, the addition/elimination pathway can give rise to the adduct IM1 (CH_3CFCH_2O) and IM2 ($CH_3CF(O)CH_2$). Under conditions from moderate to higher temperatures, IM1 will rapidly decompose to P5 (CH_3CFCHO (I) + H) and P6 (CH_3CFCHO (II) + H), and IM2 dissociates to P12 ($CH_2COF + CH_3$), which are important end products. The direct hydrogen abstraction pathway cannot compete with addition/elimination channel at low and moderate temperatures, but plays an important role at higher temperatures. Moreover, some species have been formed during the reaction, especially, formaldehyde and free radicals containing fluorine, would raise particular interest since they could effectively contribute to important radical reactions in our environment.

3.3 Kinetic calculation

For the rate constant calculations, we choose two important reaction channels: direct hydrogen abstraction and C=C bond addition/elimination. The following reaction paths are included in the calculations:

Mechanism I:

$$O(^3P) + CH_3CFCH_2 \xrightarrow{TS1a} P1{:}CH_2CFCH_2(I) + OH$$
$$\xrightarrow{TS1a} P3{:}CH_3CFCH(I) + OH.$$

Mechanism II:

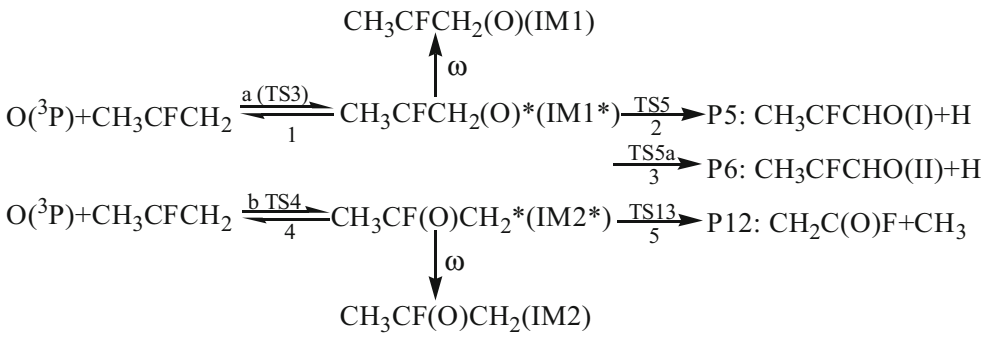

The conventional transition state theory (CTST) including the unsymmetrical Eckart tunneling correction [39] is employed to estimate the rate constants for mechanism I. For mechanism II, the multichannel RRKM–TST theory is used. During the rate constant calculations, single-point energies of all species are found at the BMC-CCSD level. The steady-state assumption for excited intermediates leads to the following expressions for the second-order rate coefficients of mechanism II:

$$k_{\mathrm{P5}}(E) = \frac{\alpha_{\mathrm{a}}}{h}\frac{Q_{\mathrm{t}}^{\neq}Q_{\mathrm{r}}^{\neq}}{Q_{\mathrm{O}(^3\mathrm{P})}Q_{\mathrm{CH_3CFCH_2}}}\mathrm{e}^{-Ea/(RT)} \times \int_0^{\infty}\frac{k_2(E)N_2(E^{\neq})}{k_1+k_2+k_3+\omega}\mathrm{e}^{-E^{\neq}/RT}\mathrm{d}E^{\neq}$$

$$k_{\mathrm{P6}}(E) = \frac{\alpha_{\mathrm{a}}}{h}\frac{Q_{\mathrm{t}}^{\neq}Q_{\mathrm{r}}^{\neq}}{Q_{\mathrm{O}(^3\mathrm{P})}Q_{\mathrm{CH_3CFCH_2}}}\mathrm{e}^{-Ea/(RT)} \times \int_0^{\infty}\frac{k_3(E)N_2(E^{\neq})}{k_1+k_2+k_3+\omega}\mathrm{e}^{-E^{\neq}/RT}\mathrm{d}E^{\neq}$$

$$k_{\mathrm{P12}}(E) = \frac{\alpha_{\mathrm{b}}}{h}\frac{Q_{\mathrm{t}}^{\neq}Q_{\mathrm{r}}^{\neq}}{Q_{\mathrm{O}(^3\mathrm{P})}Q_{\mathrm{CH_3CFCH_2}}}\mathrm{e}^{-Ea/(RT)} \times \int_0^{\infty}\frac{k_3(E)N_2(E^{\neq})}{k_4+k_5+\omega}\mathrm{e}^{-E^{\neq}/RT}\mathrm{d}E^{\neq}$$

$$k_{\mathrm{IM1}}(E) = \frac{\alpha_{\mathrm{a}}}{h}\frac{Q_{\mathrm{t}}^{\neq}Q_{\mathrm{r}}^{\neq}}{Q_{\mathrm{O}(^3\mathrm{P})}Q_{\mathrm{CH_3CFCH_2}}}\mathrm{e}^{-Ea/(RT)} \times \int_0^{\infty}\frac{w_2(E)N_2(E^{\neq})}{k_1+k_2+k_3+\omega}\mathrm{e}^{-E^{\neq}/RT}\mathrm{d}E^{\neq}$$

$$k_{\mathrm{IM2}}(E) = \frac{\alpha_{\mathrm{b}}}{h}\frac{Q_{\mathrm{t}}^{\neq}Q_{\mathrm{r}}^{\neq}}{Q_{\mathrm{O}(^3\mathrm{P})}Q_{\mathrm{CH_3CFCH_2}}}\mathrm{e}^{-Ea/(RT)} \times \int_0^{\infty}\frac{w_2(E)N_2(E^{\neq})}{k_4+k_5+\omega}\mathrm{e}^{-E^{\neq}/RT}\mathrm{d}E^{\neq}$$

$$k_{\mathrm{II}}(E) = \frac{\alpha_{\mathrm{a}}}{h}\frac{Q_{\mathrm{t}}^{\neq}Q_{\mathrm{r}}^{\neq}}{Q_{\mathrm{O}(^3\mathrm{P})}Q_{\mathrm{CH_3CFCH_2}}}\mathrm{e}^{-Ea/(RT)} \times \int_0^{\infty}\frac{(k_2+k_3+k_5+w)(E)N_2(E^{\neq})}{k_1+k_2+k_3+k_4+k_5+\omega}\mathrm{e}^{-E^{\neq}/RT}\mathrm{d}E^{\neq}.$$

In the above equations, α is the statistical factor (degeneracy) for the association step a and b; E_{a} is the energy barrier of TS3 and TS4 for the reaction step a and b; $Q_{\mathrm{O}(^3\mathrm{P})}$and $Q_{\mathrm{CH_3CFCH_2}}$ are the total partition functions of O(^{3}P) and CH_3CFCH_2, respectively; and $Q_{\mathrm{t}}^{\neq}$ and $Q_{\mathrm{r}}^{\neq}$ are the translational and rotational partition functions of the transition state TS3 and TS4 for the association. $N_2(E^{\neq})$ is the number of states for the association transition state (TS3 and TS4) with excess energy $E^{\neq}$ above the association barrier.

The microcanonical rate constant is calculated using the RRKM theory as follows:

$$k_i(E) = \alpha_i\kappa\sqrt{\frac{I_i^{\neq}}{I_j^{\mathrm{IM}}}}\frac{N_i\left(E-E_i^{\neq}\right)}{h\rho_j(E)}, \quad i=1,2,3;\ j=1,2$$

where $k_i(E)$ is the energy-specific rate constant for the ith channel; α_i is the statistical factor for reaction path degeneracy; κ is the tunneling factor; $I_i^{\neq}$ and I_j^{IM} are the moments of inertia ($I_{\mathrm{a}}I_{\mathrm{b}}I_{\mathrm{c}}$, that is, the product of I_{a}, I_{b}, and I_{c}) of the transition state i and the intermediate j; h is Planck's constant; $\rho_j(E)$ is the density of states at energy E of the intermediate j; $N_{\mathrm{i}}(E-E_i^{\neq})$ is the number of states at the energy above the barrier height for transition state i; and the density of states and the number of states are calculated using the extended Beyer–Swinehart algorithm [40, 41]. The collision deactivation rate $\omega = \beta_{\mathrm{c}}Z_{\mathrm{LJ}}[M]$; in here, β_{c} is the collision efficiency calculated using Troe's weak collision approximation [42] with the energy transfer parameter $-\langle\Delta E\rangle$. The simple expression for collisional energy transfer ($-\langle\Delta E\rangle$) [45, 46] is

$$\frac{\beta_{\mathrm{c}}}{1-\beta_{\mathrm{c}}^{1/2}} \cong \frac{-\langle\Delta E\rangle}{F_{\mathrm{E}}kT}.$$

This expression holds nearly exactly at the weak collision limit $-\langle\Delta E\rangle \ll F_E kT$ for all collision models [45, 46]. The factor F_{E} is set to 1.0 empirically. The $-\langle\Delta E\rangle$ is unknown and cannot be calculated quantitatively. In consideration of the experimental rate constants, it is found that the values around 100 cm^{-1} for $-\langle\Delta E\rangle$ should be reasonable to calculate the rate constants. Z_{LJ} is the Lennard–Jones collision frequency. The collision efficiency is estimated using the Lennard–Jones potential ($V(r) = 4\varepsilon[(\sigma/r)^{12} - (\sigma/r)^6]$) by fitting the interaction energies calculated at the MP2/6-311G(d,p) level for IM1…He and IM2…He. It is estimated that (ε = 92.2 K, σ = 4.01 Å) for IM1…He and (ε = 70.28 K, σ = 3.96 Å) for IM2…He, and [M] is the concentration of the bath gas M (He). The weak collision approximation is used for the intermediate.

The rate constants for hydrogen abstraction can be readily obtained using the conventional TST:

$$k_{\mathrm{abs}}(T) = \kappa\frac{k_{\mathrm{B}}T}{h}\frac{Q_{\mathrm{TS}}^{\neq}}{Q_{\mathrm{O}(^3\mathrm{P})}Q_{\mathrm{CH_3CFCH_2}}}\mathrm{e}^{-E/(RT)}$$

where κ is the tunneling factor and k_{B} and h are Boltzmann and Planck's constants, respectively. $Q_{\mathrm{TS}}^{\neq}$, $Q_{\mathrm{O}(^3\mathrm{P})}$, and $Q_{\mathrm{CH_3CFCH_2}}$ are the transition states (TS1a or TS1b) and OH and CH_3CFCH_2 partition functions. E is the energy barrier of the transition states (TS1a or TS1b).

For the multichannel reaction of O (^{3}P) + CH_3CFCH_2, at the bath gas of He, the calculated rate constant for direct hydrogen abstraction (H_a and H_c) from CH_3 and CH_2 group is denoted k_{TS1a} and k_{TS1b}, and the rate constant for addition/elimination is denoted k_{IM1}, k_{IM2}, k_{P5}, k_{P6}, k_{P12}, representing the rate constants of IM1, IM2, P5, P6, and P12, respectively. The total second-order rate constant for the O(^{3}P) + CH_3CFCH_2 reaction is denoted k_{tot}, $k_{tot} = k_{TS1a} + k_{TS1b} + k_{IM1} + k_{IM2} + k_{P5} + k_{P6} + k_{P12}$, and the product branching ratios are k_{TS1a}/k_{tot}, k_{TS1b}/k_{tot}, k_{IM1}/k_{tot}, k_{IM2}/k_{tot}, k_{P5}/k_{tot}, k_{P6}/k_{tot}, k_{P12}/k_{tot}, respectively. The k_{tot}(a) is obtained by high-level single-point CCSD(T)/aug-cc-pVTZ//MP2/6-311++G(d,p).

Figure 4 and Table 2 depict the total and individual rate constants over the temperature range of 200–3,000 K at the pressure of 10 Torr of He to compare with the previous experimental result. The calculated k_{tot} at BMC-CCSD level is in good agreement with experiment data; however, the values of CCSD(T)/aug-cc-pVTZ are lower than experimental rate constant and the values calculated by BMC-CCSD. As shown in Table 2, for example, at $T = 298$ K, the rate constants are 4.80×10^{-13}, 8.48×10^{-13}, and 1.99×10^{-12}cm^3 molecule^{-1} s^{-1} at the CCSD(T)/aug-cc-pVTZ, BMC-CCSD and experiment value, respectively. This is because the rate constant is determined mainly by the barrier height, especially the entrance barrier for addition step. For the formation of IM1 and IM2, the entrance barrier at BMC-CCSD level is 0.57 and 0.88 kcal/mol lower than that of CCSD(T)/aug-cc-pVTZ, which leads to the rate constant decreasing with the temperature increasing. The two sets of rate constants at these levels are in good accordance with each other in the wide temperature range. As seen in Fig. 4, the total rate constants of the title reaction show positive temperature dependence at the whole temperature region (200–3,000 K). The predicted total rate constant at 298 K is in good agreement with the available experimental data. The rate constants for direct hydrogen abstraction and addition/elimination channel increase monotonically, as well as the rate constants of IM1 and IM2 collisional stabilization channel decrease with rising temperatures. The branching ratios are shown in Fig. 5. Under 10 Torr He, the yield of P5 sharply drops with increasing temperatures, 79.6 to 29.9% between 200 and 3,000 K, whereas the yields of P6 and P12 rise with increasing temperatures first (at the 200–1,600 K), but drop with increasing temperatures ($T \geq 1{,}700$ k), and the branching ratios of P6 and P12 are smaller than that of P5 at the whole temperatures range. As can be seen in Fig. 5, the k_{TS1b}/k_{tot}, k_{IM1}/k_{tot}, k_{IM2}/k_{tot} are approximately zero at $T < 2{,}000$ K, and therefore, the contribution of P3, IM1, and IM2 can be negligible. However, the k_{TS1a}/k_{tot} almost become a constant (zero) first and then quickly increase when temperatures are greater than 2.000 K. But k_{TS1a}/k_{tot} is still lower than k_{P5}/k_{tot}. Thus, the title reaction is dominated by addition/elimination channel and the major products is P5 (CH_3CFCHO(I) + H) at low and high temperatures.

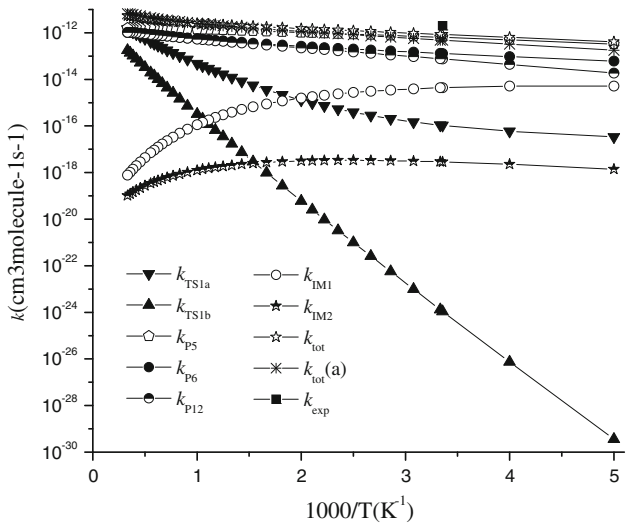

Fig. 4 Temperature dependence of the total and individual rate constants for the O(^{3}P) + CH_3CFCH_2 reaction in the temperature range 200–3,000 K at 10 Torr pressure of He along with experimental value

We also select the temperature of 298 K and perform the pressure dependence of the rate constants for addition/elimination channel. Obviously, the overall rate constant k_{II} is pressure independent at pressure range from 10^{-4} to 10^{13} Torr. However, the individual rate constants are sensitive to pressure (e.g., k_{P5} and k_{IM1} are pressure dependence). Moreover, IM1 deactivation is dominant at $P > 10^4$ Torr. Figure 6 shows that k_{IM1} exhibits positive pressure dependence when pressure is lower than 10^4 Torr, and it is a constant above 10^5 Torr when it is close to the k_{II}. k_{IM2} are much smaller than k_{IM1} at the whole pressure range(10^{-4}–10^{13} Torr). In contrast to k_{IM1}, k_{P5} is negative pressure dependence above 10^3 Torr, and it also becomes a constant below 10^3 Torr. The rate constants for P6 and P12 are always a few orders of magnitude lower than P5 and thus are negligible. At $P = 10^3$ Torr, the rate constants for k_{IM1} and k_{P5} almost take the same value. These results indicate that the stabilization k_{IM1} plays an important role in higher pressures, and the k_{P5} is dominant at low and moderate pressures.

An unsymmetrical Eckart potential was used to calculate the tunneling factor κ. For the addition mechanism, the κ was always in the range 1.2–1.0 from 200 to 3,000 K. For the main direct abstraction step, the κ is relatively large at the low temperatures. The values of κ at 200, 300, and 500 K are 8.4×10^5, 622, and 8.8, respectively. However, this significant tunneling effect cannot influence our kinetic calculations significantly. For example, at 200 K, even if

Table 2 The rate constants of k_{TS1a}, k_{TS1b}, k_{P5}, k_{P6}, k_{P12}, k_{IM1}, k_{IM2}, and total rate constants k (in cm^3 $molecule^{-1}$ s^{-1}) calculated using the TST and multichannel RRKM methodologies for the $O(^3P) + CH_3CFCH_2$ reaction between 200 and 3,000 K together with available experimental data

T (K)	k_{TS1a}	k_{TS1b}	k_{P5}	k_{P6}	k_{P12}	k_{IM1}	k_{IM2}	k_{tot}	k_{tot}(a)	k_{exp}
200	3.36×10^{-17}	3.64×10^{-30}	3.30×10^{-13}	6.05×10^{-14}	1.86×10^{-14}	5.23×10^{-15}	1.38×10^{-18}	4.14×10^{-13}	1.76×10^{-13}	
250	5.86×10^{-17}	7.41×10^{-27}	4.99×10^{-13}	9.58×10^{-14}	4.37×10^{-14}	5.13×10^{-15}	2.28×10^{-18}	6.44×10^{-13}	3.24×10^{-13}	
298	1.05×10^{-16}	1.10×10^{-24}	6.40×10^{-13}	1.29×10^{-13}	7.49×10^{-14}	4.42×10^{-15}	2.89×10^{-18}	8.48×10^{-13}	4.80×10^{-13}	1.99×10^{-12}
300	1.08×10^{-16}	1.32×10^{-24}	6.45×10^{-13}	1.31×10^{-13}	7.63×10^{-14}	4.38×10^{-15}	2.91×10^{-18}	8.57×10^{-13}	4.86×10^{-13}	
325	1.48×10^{-16}	9.93×10^{-24}	7.10×10^{-13}	1.48×10^{-13}	9.43×10^{-14}	3.95×10^{-15}	3.11×10^{-18}	9.56×10^{-13}	5.69×10^{-13}	
350	2.04×10^{-16}	5.69×10^{-23}	7.68×10^{-13}	1.65×10^{-13}	1.13×10^{-13}	3.51×10^{-15}	3.25×10^{-18}	1.05×10^{-12}	6.53×10^{-13}	
375	2.82×10^{-16}	2.61×10^{-22}	8.23×10^{-13}	1.82×10^{-13}	1.32×10^{-13}	3.10×10^{-15}	3.33×10^{-18}	1.14×10^{-12}	7.36×10^{-13}	
400	3.89×10^{-16}	1.00×10^{-21}	8.72×10^{-13}	1.99×10^{-13}	1.51×10^{-13}	2.73×10^{-15}	3.36×10^{-18}	1.23×10^{-12}	8.19×10^{-13}	
425	5.33×10^{-16}	3.31×10^{-21}	9.18×10^{-13}	2.15×10^{-13}	1.70×10^{-13}	2.38×10^{-15}	3.34×10^{-18}	1.31×10^{-12}	9.01×10^{-13}	
450	7.24×10^{-16}	9.62×10^{-21}	9.60×10^{-13}	2.32×10^{-13}	1.89×10^{-13}	2.08×10^{-15}	3.30×10^{-18}	1.38×10^{-12}	9.82×10^{-13}	
475	9.74×10^{-16}	2.52×10^{-20}	9.98×10^{-13}	2.48×10^{-13}	2.08×10^{-13}	1.81×10^{-15}	3.23×10^{-18}	1.46×10^{-12}	1.06×10^{-12}	
500	1.29×10^{-15}	6.01×10^{-20}	1.03×10^{-12}	2.65×10^{-13}	2.27×10^{-13}	1.57×10^{-15}	3.14×10^{-18}	1.52×10^{-12}	1.14×10^{-12}	
550	2.21×10^{-15}	2.74×10^{-19}	1.10×10^{-12}	2.97×10^{-13}	2.63×10^{-13}	1.18×10^{-15}	2.94×10^{-18}	1.66×10^{-12}	1.30×10^{-12}	
600	3.59×10^{-15}	9.81×10^{-19}	1.15×10^{-12}	3.29×10^{-13}	2.98×10^{-13}	8.91×10^{-16}	2.71×10^{-18}	1.78×10^{-12}	1.45×10^{-12}	
650	5.57×10^{-15}	2.92×10^{-18}	1.20×10^{-12}	3.60×10^{-13}	3.32×10^{-13}	6.74×10^{-16}	2.48×10^{-18}	1.90×10^{-12}	1.59×10^{-12}	
700	8.28×10^{-15}	7.49×10^{-18}	1.24×10^{-12}	3.90×10^{-13}	3.65×10^{-13}	5.12×10^{-16}	2.25×10^{-18}	2.00×10^{-12}	1.74×10^{-12}	
750	1.19×10^{-14}	1.71×10^{-17}	1.28×10^{-12}	4.19×10^{-13}	3.97×10^{-13}	3.91×10^{-16}	2.04×10^{-18}	2.11×10^{-12}	1.88×10^{-12}	
800	1.65×10^{-14}	3.52×10^{-17}	1.31×10^{-12}	4.48×10^{-13}	4.27×10^{-13}	3.01×10^{-16}	1.85×10^{-18}	2.20×10^{-12}	2.01×10^{-12}	
850	2.22×10^{-14}	6.72×10^{-17}	1.34×10^{-12}	4.76×10^{-13}	4.56×10^{-13}	2.33×10^{-16}	1.68×10^{-18}	2.29×10^{-12}	2.14×10^{-12}	
900	2.92×10^{-14}	1.20×10^{-16}	1.37×10^{-12}	5.03×10^{-13}	4.84×10^{-13}	1.82×10^{-16}	1.52×10^{-18}	2.39×10^{-12}	2.27×10^{-12}	
950	3.75×10^{-14}	2.01×10^{-16}	1.39×10^{-12}	5.29×10^{-13}	5.11×10^{-13}	1.44×10^{-16}	1.38×10^{-18}	2.47×10^{-12}	2.40×10^{-12}	
1,000	4.72×10^{-14}	3.22×10^{-16}	1.41×10^{-12}	5.54×10^{-13}	5.37×10^{-13}	1.14×10^{-16}	1.25×10^{-18}	2.55×10^{-12}	2.52×10^{-12}	
1,100	7.11×10^{-14}	7.31×10^{-16}	1.45×10^{-12}	6.01×10^{-13}	5.86×10^{-13}	7.35×10^{-17}	1.04×10^{-18}	2.71×10^{-12}	2.77×10^{-12}	
1,200	1.01×10^{-13}	1.46×10^{-15}	1.48×10^{-12}	6.45×10^{-13}	6.32×10^{-13}	4.88×10^{-17}	8.64×10^{-19}	2.86×10^{-12}	3.02×10^{-12}	
1,300	1.37×10^{-13}	2.63×10^{-15}	1.50×10^{-12}	6.86×10^{-13}	6.74×10^{-13}	3.33×10^{-17}	7.27×10^{-19}	3.00×10^{-12}	3.24×10^{-12}	
1,400	1.80×10^{-13}	4.37×10^{-15}	1.52×10^{-12}	7.23×10^{-13}	7.13×10^{-13}	2.34×10^{-17}	6.17×10^{-19}	3.14×10^{-12}	3.48×10^{-12}	
1,500	2.29×10^{-13}	6.83×10^{-15}	1.54×10^{-12}	7.58×10^{-13}	7.49×10^{-13}	1.68×10^{-17}	5.28×10^{-19}	3.28×10^{-12}	3.71×10^{-12}	
1,600	2.83×10^{-13}	1.01×10^{-14}	1.56×10^{-12}	7.91×10^{-13}	7.83×10^{-13}	1.23×10^{-17}	4.55×10^{-19}	3.43×10^{-12}	3.94×10^{-12}	
1,700	3.43×10^{-13}	1.43×10^{-14}	1.57×10^{-12}	8.21×10^{-13}	8.16×10^{-13}	9.26×10^{-18}	3.95×10^{-19}	3.56×10^{-12}	4.17×10^{-12}	
1,800	4.08×10^{-13}	1.96×10^{-14}	1.58×10^{-12}	8.50×10^{-13}	8.46×10^{-13}	7.09×10^{-18}	3.46×10^{-19}	3.70×10^{-12}	4.39×10^{-12}	
2,000	5.52×10^{-13}	3.35×10^{-14}	1.61×10^{-12}	9.02×10^{-13}	9.01×10^{-13}	4.37×10^{-18}	2.70×10^{-19}	4.00×10^{-12}	4.86×10^{-12}	
2,200	7.11×10^{-13}	5.24×10^{-14}	1.62×10^{-12}	9.48×10^{-13}	9.51×10^{-13}	2.86×10^{-18}	2.16×10^{-19}	4.28×10^{-12}	5.32×10^{-12}	
2,400	8.84×10^{-13}	7.62×10^{-14}	1.64×10^{-12}	9.88×10^{-13}	9.93×10^{-13}	1.96×10^{-18}	1.77×10^{-19}	4.58×10^{-12}	5.77×10^{-12}	
2,600	1.07×10^{-12}	1.05×10^{-13}	1.64×10^{-12}	1.02×10^{-12}	1.03×10^{-12}	1.40×10^{-18}	1.46×10^{-19}	4.87×10^{-12}	6.16×10^{-12}	
2,800	1.26×10^{-12}	1.39×10^{-13}	1.63×10^{-12}	1.03×10^{-12}	1.04×10^{-12}	1.03×10^{-18}	1.22×10^{-19}	5.10×10^{-12}	6.47×10^{-12}	
3,000	1.46×10^{-12}	1.78×10^{-13}	1.58×10^{-12}	1.02×10^{-12}	1.04×10^{-12}	7.77×10^{-19}	1.02×10^{-19}	5.28×10^{-12}	6.62×10^{-12}	

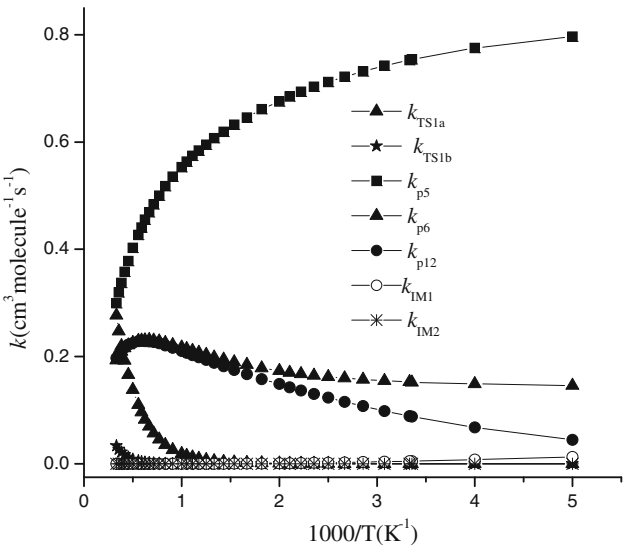

Fig. 5 Branching ratios of the important product channels for the $O(^3P) + CH_3CFCH_2$ reaction in the temperature range 200–3,000 K at 10 Torr pressure of He

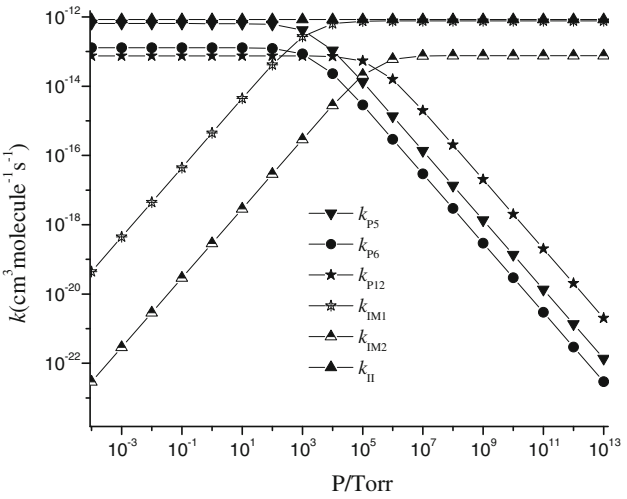

Fig. 6 Pressure dependence of the rate constants for addition/elimination channel of the $O(^3P) + CH_3CFCH_2$ reaction in the 10^{-4}–10^{13} Torr with He bath gas at 298 K

the tunneling correction is included, the dominant channel is still the addition with a rate of 4.14×10^{-13} cm^3 molecule^{-1} s^{-1} because this value is about 4 orders of magnitude higher than that for the abstraction pathway (about 3.36×10^{-17} cm^3 molecule^{-1} s^{-1}). From 1,000 to 3,000 K, κ is in the range 1.7–1.1. It is indicated that the tunneling effect is not significant at higher temperatures.

4 Conclusion

In the present study, the triplet potential energy surface for the $O(^3P) + CH_3CFCH_2$ was characterized using the high-level quantum chemical BMC-CCSD method. The rate calculations, to quantificationally predict the major products, were carried out using RRKM–TST theory. Two reaction mechanisms including H-abstraction and addition–elimination were revealed for the $O(^3P) + CH_3CFCH_2$ reaction on the triplet surface, and the addition/elimination channel was determined to be the most favorable. The title reaction exhibited both positive temperature dependence and pressure independence. At low and high temperatures, the CH_3CFCHO(I) and H were the most important products. It was worth noting the theoretical results of geometries, frequencies, and rate constants were in good agreement with experimental data. The present work would provide useful information for understanding the processes of oxygen atom reaction with other unsaturated hydrocarbons.

Acknowledgments This work supported by the National Natural Science Foundation of China (Project Nos. 20773021) and Postgraduate Innovation Fund sponsored by Northeast Normal University (No. 09SSXT121) is gratefully acknowledged. The authors are thankful for the reviewer's invaluable comments.

References

1. Farman JD, Gardiner BG, Shanklin JD (1985) Nature 315:207
2. Molina MJ, Rowland FS (1974) Nature 249:810
3. Wallington TJ, Schneider WF, Sehested J, Nielsen OJ (1995) Faraday Discuss 100:55
4. Jursic BS (1999) J Mol Struct Theochem 492:85
5. Endo Y, Tsuchiya S, Yamada C, Hirota E (1986) J Chem Phys 85:4446
6. Knyazev VD, Arutynov VS, Vedeneev VI (1992) Int J Chem Kinet 24:545
7. Gary DD, James AD (2007) J Phys Chem A 111:12977
8. Thanh LN, Lue V (2006) J Phys Chem A 110:6696
9. Thanh LN, Jozef P, Lue V (2006) J Phys Chem A 110:12166
10. Zhang WC, Du BN, Feng CJ (2007) J Mol Struct Theochem 21:806
11. Zhang YJ, Sun JY, Chao K (2011) Comput Theor Chem 965:68–83
12. Du BN, Feng CJ, Zhang WC, Mu LL (2009) Chem Phys 367:52
13. Zhou CW, Li ZR, Li XY (2009) J Phys Chem A 113:2372–2382
14. Lee SY, Yoo HS, Kang WK (1996) Chem Phys Lett 257:415
15. Young RA, Blauer J, Bower R (1988) J Chem Phys 88:4834
16. Cvetanovic RJ (1987) J Phys Chem Ref Data 16:261
17. Cometto PM, Teruel MA, Taccone RA (2006) Chem Phys Lett 417:480
18. Cometto PM, Teruel MA, Taccone RA (2005) J Phys Org Chem 18:142
19. Chemical kinetics database on the Web public beta release1.1—standard reference database 17, version 7.1, NIST standard reference data. NIST, Gaithersburg 2003 (Web Version)
20. Frisch MJ, Trucks GW, Schlegel HB, Scuseria GE, Robb MA, Cheeseman JR, Montgomery JA Jr, Vreven T, Kudin KN, Burant JC, Millam JM, Iyengar SS, Tomasi J, Barone V, Mennucci B, Cossi M, Scalmani G, Rega N, Petersson GA, Nakatsuji H, Hada M, Ehara M, Toyota K, Fukuda R, Hasegawa J, Ishida M, Nakajima T, Honda Y, Kitao O, Nakai H, Klene M, Li X, Knox JE,

Hratchian HP, Cross JB, Bakken V, Adamo C, Jaramillo J, Gomperts R, Stratmann RE, Yazyev O, Austin AJ, Cammi R, Pomelli C, Ochterski JW, Ayala PY, Morokuma K, Voth GA, Salvador P, Dannenberg JJ, Zakrzewski VG, Dapprich S, Daniels AD, Strain MC, Farkas O, Malick DK, Rabuck AD, Raghavachari K, Foresman JB, Ortiz JV, Cui Q, Baboul AG, Clifford S, Cioslowski J, Stefanov BB, Liu G, Liashenko A, Piskorz P, Komaromi I, Martin RL, Fox DJ, Keith T, Al-Laham MA, Peng CY, Nanayakkara A, Challacombe M, Gill PMW, Johnson B, Chen W, Wong MW, Gonzalez C, Pople JA (2004) Gaussian 03, revision B.03. Gaussian, Wallingford

21. MØller C, Plesset MS (1934) Phys Rev 46:61
22. Gonzalez C, Schlegel HB (1989) J Chem Phys 90:2154
23. Gonzalez C, Schlegel HB (1990) J Phys Chem 94:5523
24. Raghavachari K, Trucks GW, Pople JA, Head-Gordon M (1989) Chem Phys Lett 157:479
25. Lynch BJ, Zhao Y, Truhlar DG (2005) J Phys Chem A 109:1643
26. Baboul AG, Curtiss LA, Redfern PC, Raghavachari K (1999) J Chem Phys 110:7650
27. Moehlmann JG, Gleaves JT, Hudgens JW (1974) J Chem Phys 60:4790–4799
28. Sun JY, Tang YZ, Sun H, Jia XJ, Pan XM, Wang RS (2010) J Comput Chem 31:1126
29. Sun JY, Tang YZ, Jia XJ, Wang F, Sun H, Wang RS (2010) J Chem Phys 132:064301
30. Sun JY, Tang YZ, Sun H, Pan YR, Jia XJ, Wang RS (2008) Chem Phys Lett 463:315
31. Lee TJ, Taylor PR (1989) Int J Quantum Chem S23:199
32. Peiró-García J, Nebot-Gil I (2003) Chem Phys Chem 4:843
33. Peiró-García J, Nebot-Gil I (2003) J Comput Chem 24:1657
34. Rienstra-Kiracofe JC, Allen WD, Schaefer HF III (2000) J Phys Chem A 104:9823
35. Wang BS, Hou H, Gu YS (1999) J Phys Chem A 103:8021
36. Hou H, Li AX, Hu HY, Li YZ, Li H, Wang BS (2005) J Chem Phys 122:224304
37. Hou H, Wang BS (2007) J Chem Phys 127:054306
38. Lide DR (1993) CRC handbook of chemistry and physics, 74th edn. CRC, Boca Raton
39. Johnston HS, Heicklen J (1962) J Phys Chem 66:532
40. Stein SE, Rabinovitch BS (1973) J Chem Phys 58:2438
41. Astholz DC, Troe J, Wieters W (1979) J Chem Phys 70:5107
42. Klopman G, Joiner CM (1975) J Am Chem Soc 97:5287
43. Benjamin JL, Yan Z, Donaid GT (2005) J Phys Chem A 109:1643
44. Affefy HY, Liebman JF, Stein SE NIST ChemistryWebBook, NIST standard reference database. http://webbook.nist.gov
45. Troe J (1977) J Chem Phys 66:4745
46. Troe J (1979) J Phys Chem 83:114